THE JOURNAL OF PHYSICAL CHEMISTRY C

pubs.acs.org/JPCC

Article

Cluster-Size-Dependent Interaction between Ethylene and $CuCl_2$ Clusters Supported via γ-Alumina

Yanying Qi, Endre Fenes, Hongfei Ma, Yalan Wang, Kumar Ranjan Rout, Terje Fuglerud, Marco Piccinini, and De Chen*

Cite This: *J. Phys. Chem. C* 2020, 124, 10430−10440

Read Online

ACCESS | Metrics & More | Article Recommendations | Supporting Information

ABSTRACT: Alumina-supported copper chloride serves as an industrial catalyst for ethylene oxychlorination, resulting from its high activity and selectivity. A better understanding of the detailed active site structure and reaction mechanism is highly desired. The present work aims to explore the dependence of the structure of active sites and the adsorption of ethylene on differently sized $(CuCl_2)_n$ (n = 1−4) clusters supported by γ-Al_2O_3. The effect of the support facets (i.e., (110) and (100) surfaces) on the interface structures between the active component $CuCl_2$ and the support was also investigated. The stronger $CuCl_2$−support interaction was found on the (110) surface compared to the (100) surface, which is attributed to the stronger Lewis acidity of Al of the (110) surface. The adsorption strength of $(CuCl_2)_{n)}$ (n = 1−4) clusters becomes weak with the increment of cluster size on the (110) surface. The cluster size has a profound influence on the interaction between ethylene and the clusters. Ethylene binds to a copper atom on the small clusters (i.e., $CuCl_2$ and $(CuCl_2)_2$), while it extracts two chlorine atoms to form dichloroethane from the large clusters (i.e., $(CuCl_2)_3$ and $(CuCl_2)_4$), which explains the high activity of catalysts with high loadings upon exposure to ethylene. The effects of cluster size and alumina facets on the short d-band center and the Bader charge of the active sites result in the distinct formation energy of the chlorine vacancy and the interaction energy between C_2H_4 and the clusters. Thus, an improved catalyst could be achieved by the modification of the surface electronic structure via fine-tuning the support or adding promoters.

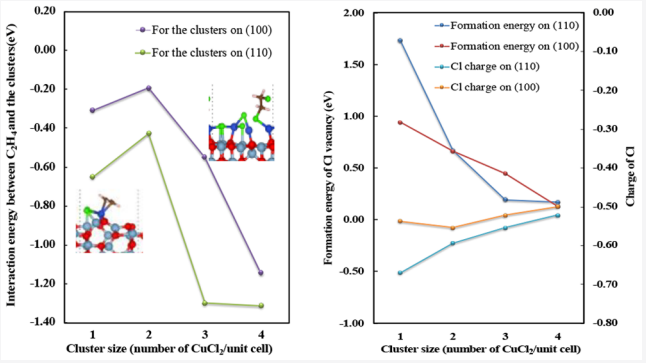

1. INTRODUCTION

Vinyl chloride monomer (VCM), which serves as the monomer for poly(vinyl chloride), is produced through the hydrochlorination of acetylene or the thermal dehydrochlorination of 1,2-dichloroethane (EDC).[1−3] EDC, in turn, is generated by direct chlorination or ethylene oxychlorination. Ethylene oxychlorination is widely used in the industry, owing to the significant economic benefits by using cheap and abundant feedback and waste HCl produced in EDC cracking. $CuCl_2$/ γ-Al_2O_3-based catalysts are effective in catalyzing ethylene, HCl, and oxygen to produce EDC in ethylene oxychlorination.[4] It has been proved that the reaction follows a three-step redox mechanism where copper is cycled by Cu(II) reduction and Cu(I) oxidation.[5−8]

$$2CuCl_2 + C_2H_4 \rightarrow 2CuCl + C_2H_4Cl_2 \quad (1)$$

$$2CuCl + 1/2O_2 \rightarrow Cu_2OCl_2 \quad (2)$$

$$Cu_2OCl_2 + 2HCl \rightarrow 2CuCl_2 + H_2O \quad (3)$$

The understanding of the detailed reaction mechanism is limited due to the complicated structure of the active site and the dynamic evolution of the active site under the reaction conditions, despite that substantial research has been devoted to investigating the nature of the active phase.[7,9−13] Lamberti and co-workers[14,15] reported that three different copper species are present: a highly dispersed copper chloride phase, a Cu−aluminate phase, and an aggregated paratacamite $(Cu_2(OH)_3Cl)$ phase. The inactive surface copper aluminate forms at low loadings, where the copper ions occupy octahedral vacancies of the alumina surface. The amorphous $CuCl_2$, formed at high loadings, is reported to be the active phase. The experimental results were analyzed by employing a defective spinel-like structure of γ-Al_2O_3 since the precise structure of γ-Al_2O_3 was unknown at the time. The intense interaction between the support and the active component is demonstrated to have a significant influence on the catalytic performance in ethylene oxychlorination.[16] Thus, employing a

Received: November 26, 2019
Revised: April 24, 2020
Published: April 24, 2020

proper γ-Al_2O_3 model is essential to acquiring the fundamental structure of the active sites. To date, it is generally agreed that γ-Al_2O_3 is a nonspinel crystal.[17,18] Based on the nonspinel model, Louwerse et al.[19] suggested that the adsorption Cu^{2+} and Cl^- are dependent on the surfaces of γ-Al_2O_3. They can adsorb on the (110) and (100) surfaces, but not on the (111) surface for the impregnated-dried catalysts at low loadings. The interaction between $CuCl_2$ and the support is still not fully resolved for the catalysts with various loadings corresponding to the distinct sizes of the active sites.

Ethylene chlorination by the reduction of $CuCl_2$ to CuCl is the first step in the redox reaction mechanism and the rate-determining step for unprompted $CuCl_2/Al_2O_3$ catalysts.[13,20] Lamberti and coworkers[6] observed that the amorphous $CuCl_2$ phase at high loadings is reduced upon the exposure to C_2H_4, but the copper aluminate at low loadings is inactive. Neurock et.al[21] reported that the adsorption model and the adsorption energy of ethylene are affected by the coordination number, the oxidation state, and the ligand at the copper center. However, the model of alumina is highly simplified due to the limitation of computational speed almost two decades ago. The exploration of ethylene adsorption behaviors on more accurate models with different cluster sizes is highly desired to understand the effects of the alumina facets and the size of the clusters on the catalytic performance.

Herein, we built up surface clusters with distinct sizes to simulate the catalyst structure at various Cu loadings. We investigated the interaction between the active site $CuCl_2$ and two γ-Al_2O_3 surfaces (i.e., nonspinel γ-Al_2O_3(110) and (100) surfaces). The effects of the support surfaces and the size of the cluster on the interaction were examined. We further explored the adsorption modes of ethylene on the various $CuCl_2/\gamma$-Al_2O_3 models with distinct cluster sizes and different support surfaces. Moreover, the analyses of the formation energy of the chorine vacancy, d-band center, and Bader charge on different structures were investigated to unravel the underlying reason for the distinct ethylene adsorption behaviors at different Cu loadings.

2. METHODS

DFT calculations were performed using the Bayesian error estimation functional with the van der Waals correlation (BEEF-vdW) functional,[22] as implemented in the VASP 5.3 code.[23−25] The projected augmented wave (PAW) method[26] combined with the plane-wave expansion at a kinetic energy cutoff of 400 eV was adopted. The Brillouin zone integration was conducted with a $4 \times 4 \times 1$ k-point grid. The ground-state atomic geometries of the bulk and surface were obtained when the total energy difference between two steps of the SCF loop was below 1×10^{-4} eV, and the residual forces on atoms were below 0.03 eV/Å. Convergence tests with a cutoff energy of 450 eV and a force convergence criterion of 0.01 eV/Å show that the adsorption energy of $CuCl_2$ was converged to less than 0.01 eV.

The nonspinel bulk structure of alumina proposed by Digne et.al[17,18] was adopted in this study. The optimized lattice parameters are a = 5.593 Å, b = 8.419 Å, c = 8.082 Å, and β = 90.545°, which are similar to the reported values.[17,27]Two preferentially exposed crystal facets, the (110) and (100) surfaces, were investigated in this study. The two surfaces account for 90% of the total surface area of γ-Al_2O_3. Besides, previous investigations suggested that Cu^{2+} and Cl^- adsorb exclusively on these two surfaces rather than the (111) surface.[19] The surfaces are simulated using a slab model with 8 atomic layers and 12 layers for the dehydrated (110) and (100) surfaces, respectively. A vacuum of 15 Å is set between two periodic repeated slabs. The total thickness of the unit cell was 29.5 and 25.0 Å for the dehydrated (100) and (110) surfaces, respectively. The sizes of the unit cells are (1×1) and (2×1) for the (110) and (100) surfaces, respectively. The detailed unit cell vectors of the model are shown in Table S1, Supporting Information. The adsorption energy of $CuCl_2$ on γ-Al_2O_3(110) with a size of (2×1) is −0.03 eV smaller than that on γ-Al_2O_3(110) with a size of (1×1). Thus, we employed the size of (1×1) here to save computational time. The bottom four layers of the (110) surface or the bottom six layers of the (100) surface were kept fixed at bulk coordinates during the calculations, whereas the top layers were allowed to relax. The calculated surface energies for (110) and (100) are 1531 and 961 mJ/m^2, respectively, which agree well with the previously reported results.[17,27] Numerous initial adsorption configurations were constructed based on chemical intuition. Different orientations were probed; especially parallel and upright were considered. The initial guesses of the adsorption of $(CuCl_2)_n$ are based on the optimum configuration of $(CuCl_2)_{n-1}$ adsorbed on the surface. The structure with the lowest total energy is selected as the most stable configuration. Frequency analysis was performed to confirm the selected stable structures. The adsorption energy of $CuCl_2$ on the alumina surface is calculated in the following equation:

$$E_{ads} = [E_{(CuCl_2)_n-Al_2O_3} - n^*E_{CuCl_2} - E_{Al_2O_3}]/n$$

where $E_{(CuCl_2)_n-Al_2O_3}$ is the total energy of the adsorbed $(CuCl_2)_n$ cluster, n is the number of $CuCl_2$ monomers in the cluster, E_{CuCl_2} is the total energy of the isolated CuCl monomer, and $E_{Al_2O_3}$ is the total energy of the optimized alumina slab. The interaction energy between ethylene and the slab is calculated as $E_{int} = E_{A+slab} - E_A - E_{slab}$, where E_A is the total energy of the C_2H_4 molecule in the gas phase, E_{slab} is the total energy of the clean surface, and E_{A+slab} is the minimum total energy of ethylene adsorbed on the slab.

Bader charge analysis[28,29] provides a useful method for assigning charge to an atom, enabling the determination of charge transfer in an adsorption system. The quality of the grid was tested to ensure the accuracy of the calculation. The difference in charge density is calculated by $\Delta\rho = \rho$(molecule + slab) $- \rho$(slab) $- \rho$(molecule), which is visualized by using the VESTA software,[30] where ρ(molecuele + slab) is the charge of the optimized structure of the molecule on the surface, ρ(slab) is the charge of the clear surface, and ρ(molecule) is the charge of free molecules.

3. RESULTS AND DISCUSSION

A systematic investigation of the interface structure between the $CuCl_2$ and the support was performed for the catalyst at different loadings. First, the relationship between the cluster size and the Cu loading of the real catalysts was built. The cluster size increases with the increment of Cu loadings, as shown in Table 1. The details of the calculation are summarized in Section S1, Supporting Information. Moreover, the structures of $CuCl_2$ on γ-Al_2O_3(110) and (100) were explored, where the $CuCl_2$ binding with different sites on the surface with different orientations was tested. All the possible configurations are summarized in Figure S1, Supporting

https://dx.doi.org/10.1021/acs.jpcc.9b11037
J. Phys. Chem. C 2020, 124, 10430−10440

Table 1. Number of $CuCl_2$ in the Cluster Model, the Corresponding Site Coverage of $CuCl_2$ on the (110) and (100) Surfaces, and the Catalyst Loadings

no. of $CuCl_2$ in the cluster model	1	2	3	4
sites converged on 110 (nm^{-2})	1.5	2.9	4.4	5.9
sites converged on 100 (nm^{-2})	1.6	3.1	4.7	6.2
Cu loading	2%	4%	6%	8%

Information, and the most stable ones are reported in Figure 1 and Figure 2.

3.1. Structures of $CuCl_2$ on the γ-Al_2O_3(110) Surface. The (110) surface is the most exposed surface of γ-Al_2O_3, accounting for 70% of the surface area of γ-Al_2O_3. The unit cell in Figure 1 presents one threefold-coordinated Al_3 site (i.e., Al_A) and three fourfold-coordinated Al_4 sites (i.e., Al_B, Al_C, Al_D), as well as three twofold-coordinated O_{II} sites (i.e., O_4, O_5, and O_6) and three threefold-coordinated O_{III} sites (i.e., O_1, O_2, and O_3). The surface Al_3, Al_4, and O_{II} sites are coordinately unsaturated while only the O_{III} sites are saturated. Numerous initial adsorption configurations of $(CuCl_2)_n$ (n = 1−4) on the γ-Al_2O_3(110) surface are constructed by adding a $CuCl_2$ molecule on the most stable $(CuCl_2)_n$ (n = 1−4) based on chemical intuition. The most stable structures are displayed in Figure 1, and the structure parameters, as well as the adsorption energies, are summarized in Table 2. It is found that the adsorption energies of $CuCl_2$ decrease with the increase in the cluster size. Besides, we compared the adsorption energy of $CuCl_2$ by using the BEEF-vdW and rPBE functionals[31] to demonstrate the effect of vdW correction

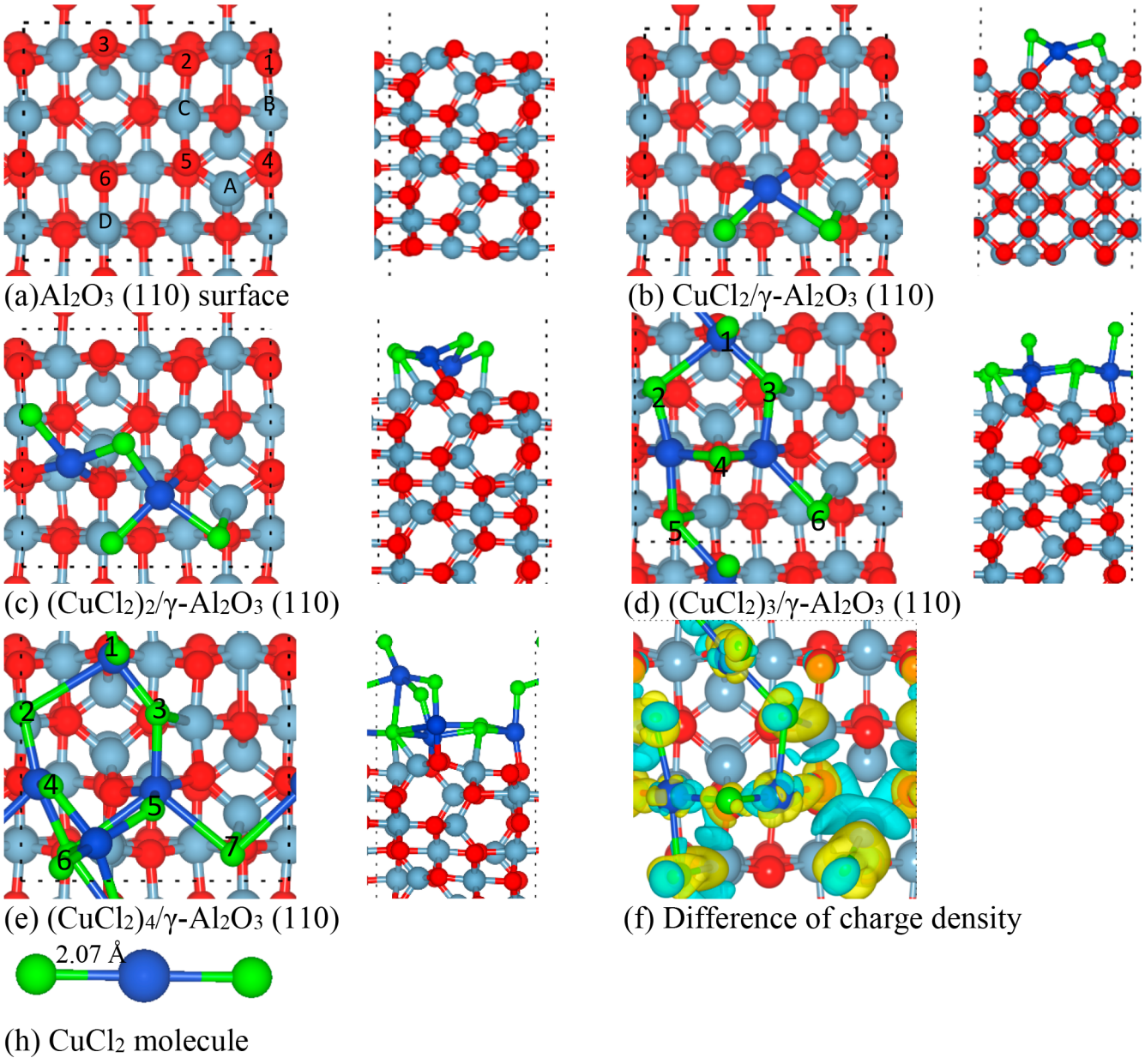

Figure 1. (a−e) Adsorption configurations of $(CuCl_2)_n$ (n = 1−4) on the γ-Al_2O_3(110) surface. Left are top views, and right are side views. (f) Difference of the charge density of $(CuCl_2)_3/\gamma$-Al_2O_3(110). (h) The original $CuCl_2$ molecule. O, red; Al, livid; Cu, blue; Cl, green. The same colors are applied in the whole paper. The chlorine atoms are labeled by number. The yellow and blue in the charge density difference picture represent the charge accumulation and depletion isosurfaces, respectively.

https://dx.doi.org/10.1021/acs.jpcc.9b11037
J. Phys. Chem. C 2020, 124, 10430−10440

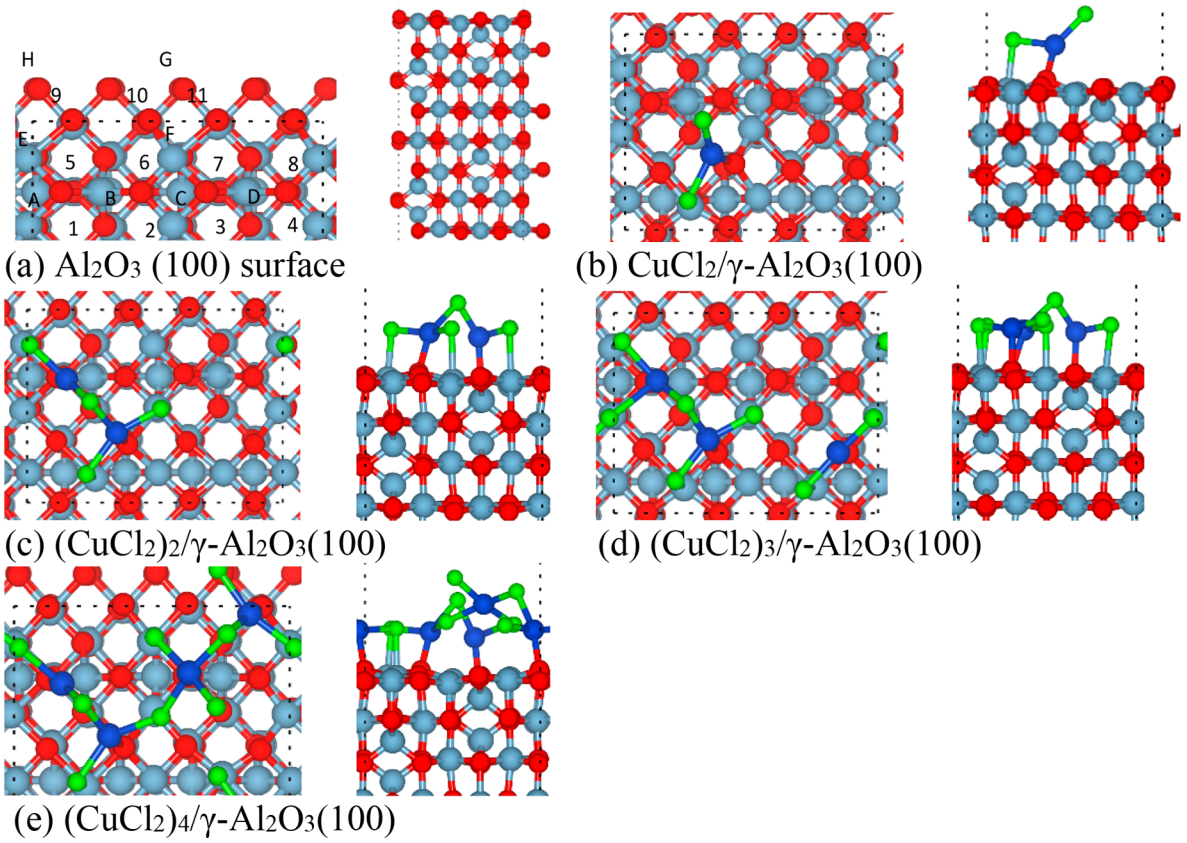

Figure 2. Adsorption configurations of $(CuCl_2)_n$ (n = 1−4) on the γ-Al_2O_3(100) surface. Left is the top view, and right is the side view.

Table 2. Adsorption Energies and Structure Parameters of $n(CuCl_2)$ (n = 1−4) on the γ-Al_2O_3(110) and γ-Al_2O_3(100) Surfaces[a]

	110			100		
$CuCl_2$ cluster	E_{ads} (eV)	d_{Cu-Cl} (Å)	$\theta_{Cl-Cu-Cl}$ (deg)	E_{ads} (eV)	d_{Cu-Cl} (Å)	$\theta_{Cl-Cu-Cl}$ (deg)
$CuCl_2$	−2.92	2.22, 2.69	97	−1.25	2.11, 2.27	117
$(CuCl_2)_2$	−2.27	2.28, 2.29	94	−1.55	2.17, 2.22	121
$(CuCl_2)_3$	−1.95	2.17, 2.34	87	−1.49	2.12, 2.16	166
$(CuCl_2)_4$	−1.77	2.17, 2.28	153	−1.39	2.19, 2.24	169

[a]Note: d_{Cu-Cl} and $\theta_{Cl-Cu-Cl}$ are the distance of Cu and Cl and the bond angle in the newly added molecule.

on the adsorption of $CuCl_2$. As summarized in Table S2, the adsorption energy of $CuCl_2$ using BEEF-vdW is larger than that with rPBE by 0.6−0.8 eV, and the adsorption energy change with the cluster size follows a similar trend for these two functionals.

$CuCl_2$ strongly adsorbs on the surface with an adsorption energy of −2.92 eV, which results in the formation of a Cu−aluminate phase and the transformation of both the $CuCl_2$ and the alumina surface, as shown in Figure 1. The original $CuCl_2$ is linear with a Cu−Cl bond length of 2.07 Å, as shown in Figure 1h. The $CuCl_2$ molecule is distorted during the optimization process; that is, $\theta_{Cl-Cu-Cl}$ changes to 97° from 180°. The copper atom strongly binds to O_5 and O_6, and the lengths of Cu−O_5 and Cu−O_6 are 1.90 and 2.02 Å, respectively. The average Cu−O length is 1.96 Å, which agrees well with experimental results (1.94 ± 0.1 Å).[14] The chlorine atoms bind to Al_A (2.18 Å) and Al_D (2.36 Å) atoms, respectively. Al_A is the strongest Lewis acid site followed by Al_D based on the calculated unoccupied s-band center,[32] and thus they strongly bind with Cl. The intense interaction between $CuCl_2$ and the surface atoms leads to the separation of one Cl atom from the molecule, where the Cu−Cl bond is elongated by 0.62 Å.

The adsorption energy of $(CuCl_2)_2$ is −2.27 eV, which is weaker than that of $CuCl_2$ since $CuCl_2$ has occupied the most unsaturated Al and O atoms. The second added $CuCl_2$ molecule is bent via a similar angle to the first one, and the Cu−Cl bonds are slightly elongated. The copper atom in the second $CuCl_2$ molecule binds to O_4 and O_6, and both the bond lengths are 1.99 Å. One chlorine atom is bound to the Al_B atom with a distance of 2.43 Å, while the other attaches to the copper atom in the first added $CuCl_2$ molecule. The interaction between the first $CuCl_2$ and the second $CuCl_2$ results in the decrease of the bond length between the copper atom and the chlorine atoms in the first $CuCl_2$ molecule.

For $(CuCl_2)_3/\gamma$-Al_2O_3(110), the third added $CuCl_2$ molecule significantly modified the structure of the first two $CuCl_2$ on the surface. One chlorine atom in the third $CuCl_2$ is bound to the first copper, which results in the bond breakage of Cu−Cl in the first $CuCl_2$ molecule. The difference of the charge density of $(CuCl_2)_3/\gamma$-Al_2O_3(110) clearly illustrates the charge transfer between the $CuCl_2$ cluster and γ-Al_2O_3(110). The charge accumulation on the Cl atoms and the charge depletion on the Cu atoms are detected. For $(CuCl_2)_4/\gamma$-Al_2O_3(110), the fourth added $CuCl_2$ molecule does not directly attach to the alumina surface, and the second layer of the $CuCl_2$ cluster appears. The Cu−Cl bonds in the fourth

https://dx.doi.org/10.1021/acs.jpcc.9b11037
J. Phys. Chem. C 2020, 124, 10430−10440

$CuCl_2$ molecule are elongated by 0.10 and 0.21 Å, which are much smaller compared to those in the first $CuCl_2$ molecule. Besides, the adsorption strength decreases with the accumulation of $CuCl_2$, which indicates that the interactions among the $CuCl_2$ molecules are weaker than those between the $CuCl_2$ molecules and the alumina surface.

3.2. Structure of $CuCl_2$ on the γ-Al_2O_3(100) Surface. The (100) surface is one of the most detected and catalytically active surfaces for anchoring deposited transition metal and metal oxide particles. In the supercell of the fully dehydrated γ-Al_2O_3(100) surface, 8 fivefold-coordinated Al_5 and 12 threefold-coordinated O_3 sites are exposed, which originate from the sixfold-coordinated bulk Al atoms and the fourfold-coordinated bulk O atoms. The first copper atom binds to the O_6 atom with a distance of 1.96 Å, and the chlorine atom binds to the Al_B atom with a length of 2.38 Å upon the adsorption of $CuCl_2$. The O_6 and Al_B atoms are pulled up due to the interaction between the alumina surface and $CuCl_2$. Similar to the adsorption mode on the (110) surface, $\theta_{Cl-Cu-Cl}$ changes to 117°, and the bonds of Cu−Cl are elongated to 2.11 and 2.27 Å. The changes of both bond angles and bond lengths are moderate, and the adsorption energy of −1.25 eV is less negative compared to that on the (110) surface, which reflects the relatively weaker interaction between the $CuCl_2$ molecule and the (100) surface. It is owing to the high degree of saturation and the weak Lewis acidity of aluminum atoms of the (100) surface.[32,33]

The adsorption energy of $(CuCl_2)_2$ is −1.55 eV, which is slightly smaller compared to the adsorption of $CuCl_2$ due to the formation of a more stable dimer. The second added $CuCl_2$ monomer is anchored to the surface by forming the bonds Cu−O_9 and Cl−Al_H. The chlorine atom binds with the copper atom in the first $CuCl_2$, which displays in the shape of a T. In the configuration of $(CuCl_2)_3$/γ-Al_2O_3(100), the third $CuCl_2$ molecule, with two Cu−Cl bond lengths of 2.12 and 2.16 Å, is parallel to the first molecule. The adsorption energy of $(CuCl_2)_3$ is similar to the adsorption of $CuCl_2$ on γ-Al_2O_3. Like the adsorption on the (110) surface, the second layer is initiated by the addition of the fourth added $CuCl_2$ molecule. The adsorption energy of $(CuCl_2)_4$/γ-Al_2O_3(100) slightly increases to −1.39 eV.

It is found that the adsorption of the $CuCl_2$ clusters on the (100) surface is weaker than that on the (110) surface, which is due to the weaker Lewis acidity of Al atoms on the (100) surface.[32,33] The stronger acidic site of the (110) surface owns the lower s-conduction band mean of the Al atom (i.e., closer to the Fermi level),[33] and thus it is easier to accept electronic charges from the Cl atoms, which results in the stronger adsorption of $CuCl_2$ on (110). Besides, the Al−O bond on the (110) surface is more compact, which also results in the strong interaction between $CuCl_2$ and the support.

Figure 3 illustrates the decrease of the adsorption strength of $CuCl_2$ on the γ-Al_2O_3(110) with the increase of the cluster size. The adsorption strength of the second $CuCl_2$ on the (100) surface is larger than that of the first one due to the formation of a stable dimer, and then the adsorption becomes weak with the increment of the cluster size. The difference in the adsorption energy of the $CuCl_2$ cluster with various sizes on the (100) surface is smaller compared to that on the (110) surface, which is attributed to the more homogeneous properties of various adsorption sites on the (100) surface.

Here, we employed the dehydrated γ-Al_2O_3(110) and (100) surfaces, whereas the structure of the γ-Al_2O_3 surfaces under realistic reaction conditions is much more complicated. At the reaction temperature 500 K, the Lewis acid surface sites (i.e., the undercoordinated Al sites) are partially occupied by hydroxyl groups. The theoretical calculated OH coverages at 500 K are 11.8 and 8.8 OH/nm^2 for the (110) surface and the (100) surface, respectively.[17,19] The adsorption energy of $CuCl_2$ on the (110) surface is −1.97 eV, which is still stronger than that on the (111) surface (i.e., −1.35 eV). The hydroxyl groups do not change the relative performance on the two different surfaces. Thus, we investigated the adsorption behavior of ethylene on the dehydrated models due to the limitation of computation time. It is noted that HCl as a reactant could result in the surface chlorination by substituting the hydroxyl groups by Cl, which depends on the relative partial pressure of HCl/H_2O and the temperature.[18,34] Besides, we found the fresh catalyst needs HCl to trigger its activity. The role of various surface species (i.e., OH, H_2O, HCl, Cl) on the catalytic performance will be exploited in our future studies.

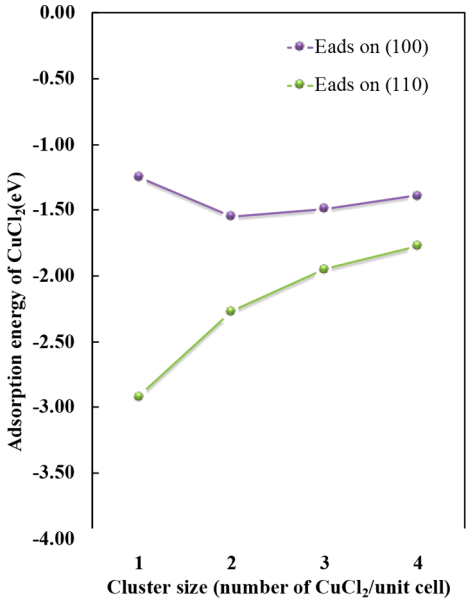

Figure 3. Size-dependent adsorption energy of $CuCl_2$ on γ-Al_2O_3(110) and (100).

3.3. C_2H_4 Adsorption on the $(CuCl_2)_n$ Cluster Supported by the γ-Al_2O_3(110) and (100) Surfaces. Ethylene adsorption is an essential step for catalyst reduction, and thus the investigation of the adsorption mode is essential to identify the nature of the active site. Herein, the adsorption geometries of ethylene on $(CuCl_2)_n$ (n = 1−4)/γ-Al_2O_3(110) and $(CuCl_2)_n$ (n = 1−4)/γ-Al_2O_3(100) are explored to elucidate the different reduction performances at various Cu loadings. Neurock et.al[21] reported that the adsorption energy of ethylene is sensitive to the orientation of ethylene at one adsorption site. Therefore, different orientations were examined, for example, ethylene sites atop the copper center with varying degrees of rotation and C═C bonds lying perpendicular or parallel to the Cu_xCl_y plane. Moreover, we examined the possibilities of ethylene binding with chlorine atoms and with the alumina surface atoms since alumina could be the catalyst in reactions such as ethanol dehydration to ethylene. All the possible configurations of ethylene adsorbing on $(CuCl_2)_n$ (n = 1−4) supported by γ-Al_2O_3(110) and (100) are summarized in Figure S2, Supporting Information.

https://dx.doi.org/10.1021/acs.jpcc.9b11037
J. Phys. Chem. C 2020, 124, 10430−10440

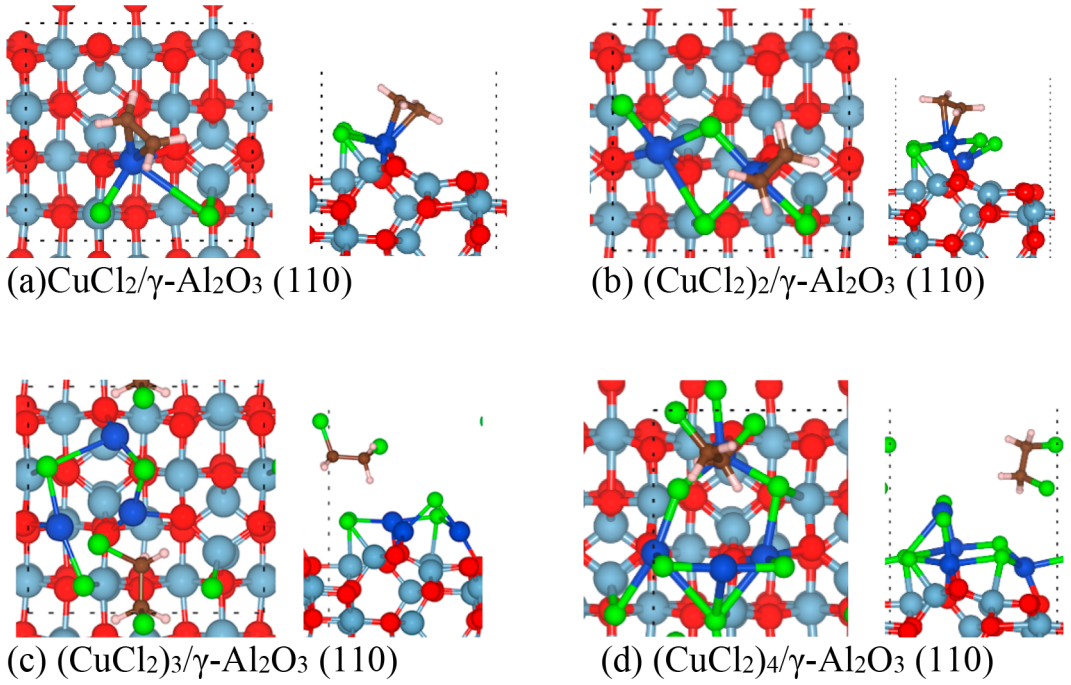

Figure 4. Top views and side views of the most stable adsorption configurations of ethylene on the $(CuCl_2)_n/\gamma\text{-}Al_2O_3(110)$ surface. C, brown; H, pink. The same colors are applied in the following sections.

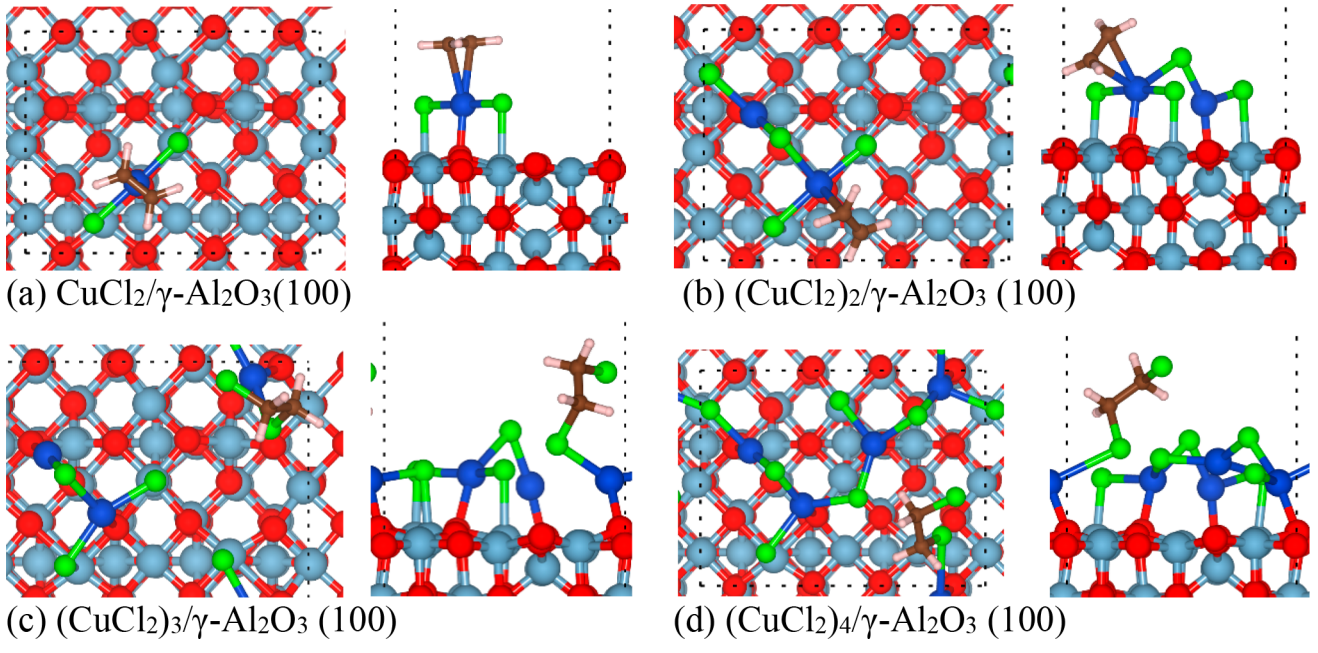

Figure 5. Top views and side views of the most stable adsorption configurations of ethylene on the $n(CuCl_2)$ $(n = 1-4)/\gamma\text{-}Al_2O_3(100)$ surface.

Ethylene cannot bind with the surface atoms of alumina, which just physically adsorb on the surface. The most stable configurations of ethylene on various clusters are illustrated in Figure 4 and Figure 5.

3.3.1. C_2H_4 Adsorption on $(CuCl_2)_n/\gamma\text{-}Al_2O_3(110)$. Ethylene is bound to the copper atom when ethylene adsorbs on the $CuCl_2$ and $(CuCl_2)_2$ clusters supported on $\gamma\text{-}Al_2O_3(110)$, which is similar to the result from Neurock et al.[21] The lengths of two Cu−C bonds are 2.19 and 2.20 Å, respectively. The Cu−Cl bonds are elongated to 2.34 and 3.52 Å upon the adsorption of ethylene, which means one Cu−Cl bond is broken upon the ethylene adsorption. The adsorption strength decreases with the increase of the size of the $CuCl_2$ cluster, which is consistent with Neurock's work.[21]

With regards to the adsorption of ethylene on $(CuCl_2)_3/\gamma\text{-}Al_2O_3(110)$ and $(CuCl_2)_4/\gamma\text{-}Al_2O_3(110)$, ethylene could also bind to one copper atom. However, it is not the most stable configuration. As shown in Figure 4, ethylene binds to two chlorine atoms and is converted to EDC by extracting two chlorine atoms from the surface in the most stable configurations. Correspondingly, the surface is significantly distorted upon the adsorption of ethylene. It is found that the distance between two neighboring chlorine atoms needs to be around 3.5 Å to make ethylene bind to two chlorine atoms

https://dx.doi.org/10.1021/acs.jpcc.9b11037
J. Phys. Chem. C 2020, 124, 10430−10440

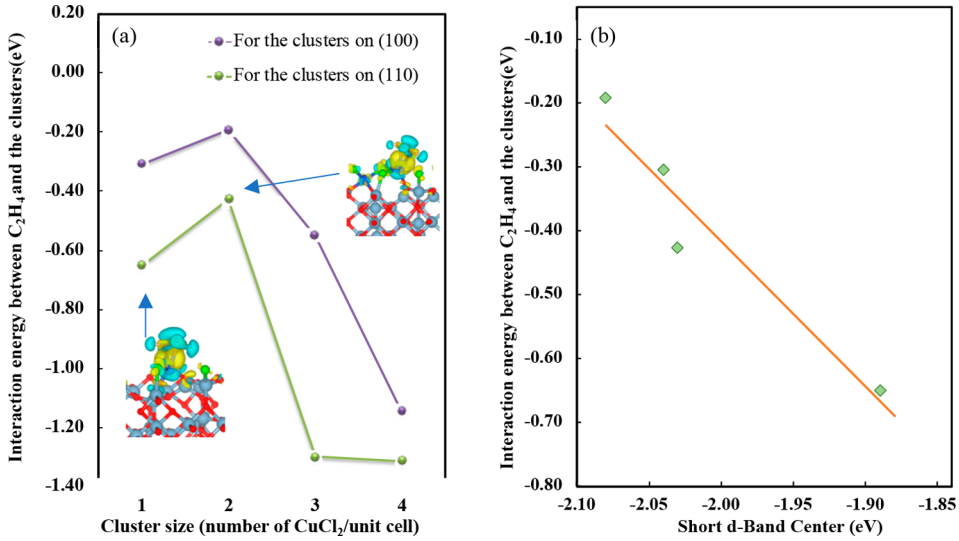

Figure 6. (a) Interaction energy between C_2H_4 and the clusters as a function of cluster size on γ-Al_2O_3(110) and (100). It is noted that ethylene binds with the copper atom on smaller clusters (i.e., $CuCl_2$ and $(CuCl_2)_2$), and EDC is formed upon the interaction between ethylene and the larger clusters (i.e., $(CuCl_2)_3$ and $(CuCl_2)_4$). (b) Interaction energy between C_2H_4 and the clusters as a function of the Cu short d-band center on $CuCl_2$ and $(CuCl_2)_2$ clusters. The two insets are the difference of charge density on $CuCl_2$ and $(CuCl_2)_2/\gamma$-Al_2O_3(110).

simultaneously. However, ethylene cannot bind to the chlorine atoms on $(CuCl_2)_2/\gamma$-Al_2O_3(110) even if there are two neighboring chlorine atoms with a distance of around 3.5 Å.

For the $(CuCl_2)_3/\gamma$-Al_2O_3(110) surface, eight possibilities for two neighboring chlorine atoms with a distance of around 3.5 Å were tested, that is, Cl_1-Cl_2, Cl_1-Cl_3, Cl_1-Cl_4, Cl_2-Cl_4, Cl_3-Cl_4, Cl_4-Cl_5, Cl_5-Cl_6, and Cl_1-Cl_5. Ethylene binds with two chlorine atoms in all the initial configurations. However, different adsorption modes are generated after optimization. The optimized configurations are summarized in Figure S3, Supporting Information. Ethylene binds to two chlorine atoms and is converted to EDC in the cases of Cl_1-Cl_2, Cl_1-Cl_5, Cl_1-Cl_4, and Cl_1-Cl_3. In the case of Cl_4-Cl_5, ethylene binds with two chlorine atoms, while the chlorine atoms also bind to the copper atoms. Ethylene cannot bind to the surface atoms in the cases of Cl_2-Cl_4, Cl_3-Cl_4, and Cl_5-Cl_6. With regards to $(CuCl_2)_4/\gamma$-Al_2O_3(110), six possibilities with two neighboring chlorine atoms were tested, which are Cl_2-Cl_4, Cl_3-Cl_5, Cl_4-Cl_5, Cl_4-Cl_6, Cl_5-Cl_7, and Cl_1-Cl_6 as shown in Figure S4, Supporting Information. Similarly, three different adsorption modes are observed after optimization. EDC forms in the cases of Cl_1-Cl_6 and Cl_4-Cl_6. No bond forms between ethylene and chlorine in the instances of Cl_3-Cl_5. The chlorine atoms bind with the carbon atom and the copper atoms in the other cases. Thus, two neighboring chlorine atoms with a distance of around 3.5 Å are not the sole requirement to obtain the stable configuration of ethylene binding with Cl atoms. Other structure parameters or electronic properties may also affect the adsorption of ethylene on the surface. For example, the chlorine atoms bind with both the aluminum atoms and the copper atoms on $CuCl_2/\gamma$-Al_2O_3(110) and $(CuCl_2)_2/\gamma$-Al_2O_3(110), while at least one of the extracted chlorine atoms exclusively binds to the copper atom on $(CuCl_2)_3/\gamma$-Al_2O_3(110) and $(CuCl_2)_4/\gamma$-Al_2O_3(110). The underlying reason is explored in Section 3.3.3.

EDC is formed upon ethylene adsorption on $(CuCl_2)_3/\gamma$-Al_2O_3(110) and $(CuCl_2)_4/\gamma$-Al_2O_3(110), which indicates that the EDC formation is an easy process. We performed temperature-programmed reduction (TPR) on the catalyst with 5% Cu loading to verify our theoretical results. The detailed procedure and the results are summarized in Section S2 and Figure S5, Supporting Information, respectively. The TPR result elucidates that EDC can be generated at around 50 °C, which demonstrates that it is an easy process.

Besides, we investigated the adsorption mode of the second ethylene on the clusters to check if EDC can still be formed at a high coverage of ethylene. The most stable configurations are summarized in Figure S6, Supporting Information. On the small-sized clusters (n = 1 and 2), the second ethylene is physically adsorbed. On the large-sized clusters, the second ethylene binds to the copper atom with much lower interaction energy between C_2H_4 and the clusters, instead of the formation of EDC. The interaction energy between the second C_2H_4 and the clusters is calculated as $E_{int} = E_{S+2C_2H_4} - E_{S+C_2H_4} - E_{C_2H_4}$, where $E_{S+2C_2H_4}$ and $E_{S+C_2H_4}$ are the total energy of two ethylenes and one ethylene adsorbed on the surface, respectively. $E_{C_2H_4}$ is the gas phase ethylene. Compared with that of the first ethylene, the adsorption of the second ethylene becomes weaker, which is due to the modification of the electronic properties of the clusters via the first adsorbed ethylene. Figure S7 illustrates that the change of interaction energy between the second C_2H_4 and the clusters with the cluster size follows a similar trend to the adsorption of the first one.

3.3.2. C_2H_4 Adsorption on $(CuCl_2)_n/\gamma$-Al_2O_3(100). Ethylene sits atop of the copper atom on $CuCl_2/\gamma$-Al_2O_3(100). The bond lengths of two C−Cu bonds (2.49 and 2.50 Å) are larger, and the interaction energy between ethylene and the cluster is smaller compared to that on $CuCl_2/\gamma$-Al_2O_3(110), which may be attributed to the weaker interaction between the $CuCl_2$ molecule and the alumina surface for γ-Al_2O_3(100). The structure of the $CuCl_2$ molecule is modified upon the adsorption of ethylene; that is, it becomes linear, and both chlorine atoms bind to the aluminum atoms. Ethylene binds to the copper atom with distances of 2.57 and 2.50 Å on $(CuCl_2)_2/\gamma$-Al_2O_3(100), which is similar to that on $CuCl_2/\gamma$-Al_2O_3(100). Ethylene extracts two chlorine atoms from the cluster and is converted to EDC in the most stable

https://dx.doi.org/10.1021/acs.jpcc.9b11037
J. Phys. Chem. C 2020, 124, 10430−10440

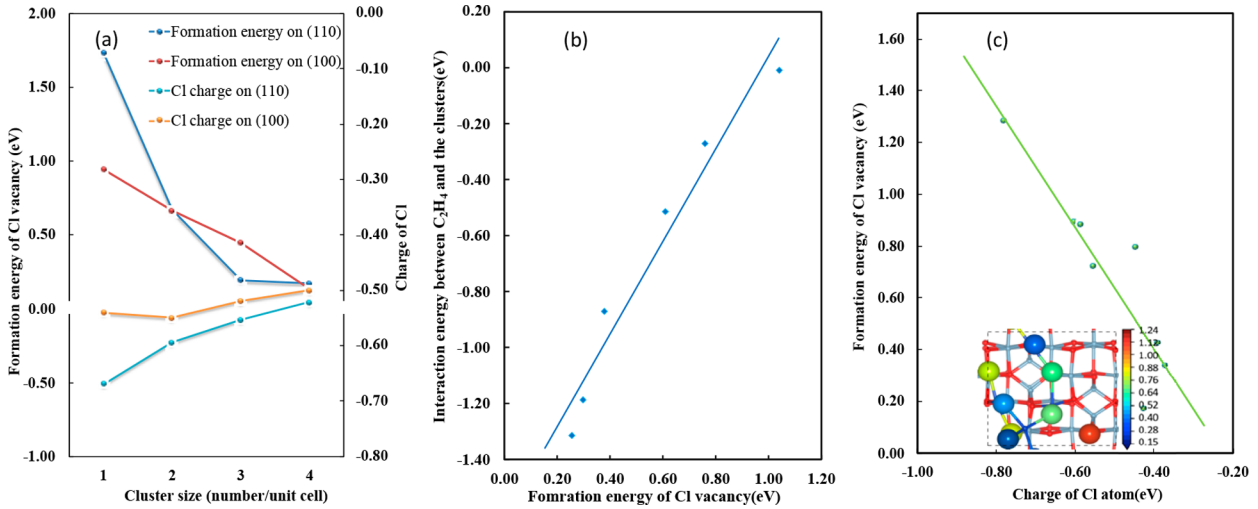

Figure 7. (a) Size-dependent formation energy of the Cl vacancy and average Bader charge of Cl. (b) Formation energy of the Cl vacancy determines the interaction modes between C_2H_4 and the clusters on $(CuCl_2)_4/\gamma$-$Al_2O_3(110)$. (c) Relationship between the formation energy of the Cl vacancy and the Bader charge of the Cl atom on $(CuCl_2)_4/\gamma$-$Al_2O_3(110)$ and the mapping of the ΔE_v of all the Cl atoms on $(CuCl_2)_4/\gamma$-Al_2O_3 (inset figure).

configurations of $(CuCl_2)_3/\gamma$-$Al_2O_3(100)$ and $(CuCl_2)_4/\gamma$-$Al_2O_3(100)$, as shown in Figure 5. However, one chlorine atom in EDC still binds with the copper atom. Eight possibilities of two neighboring chlorine atoms with a distance of around 3.5 Å were tested for $(CuCl_2)_3/\gamma$-$Al_2O_3(100)$, and ethylene could bind to two chlorine atoms in only one configuration. Fourteen possibilities were tested for $(CuCl_2)_4/\gamma$-$Al_2O_3(100)$. Three different adsorption modes are observed; that is, ethylene binds to two chlorine atoms with one chlorine atom binding to the copper atoms; two chlorine atoms bind to both ethylene and the copper atoms; and no bonds are formed between ethylene and the surface.

It is concluded that distinct adsorption modes of ethylene are observed on both $(CuCl_2)_n/\gamma$-$Al_2O_3(110)$ and $(CuCl_2)_n/\gamma$-$Al_2O_3(100)$. C_2H_4 is bound to the copper atom of the small clusters (i.e., $CuCl_2$ and $(CuCl_2)_2$), while C_2H_4 is converted to EDC by attaching to two chlorine atoms on the relatively more massive clusters (i.e., $(CuCl_2)_3$ and $(CuCl_2)_4$). Moreover, it is found that two neighboring chlorine atoms with a distance of around 3.5 Å are not the sole requirement to obtain the stable configuration of ethylene binding with Cl atoms.

Leofanti et al. investigated the effect of exposure to C_2H_4 on $CuCl_2/Al_2O_3$ catalysts with different Cu loadings. They observed that the catalyst with a Cu loading of 1.4% is inactive in ethylene conversion to dichloroethane and the catalyst with Cu loading of 9.0% shows high activity.[6] At low loadings, the copper surface aluminate phase is formed, and the catalyst is difficult to be reduced, which is demonstrated by the strong binding between $CuCl_2$ and Al_2O_3 at low $CuCl_2$ coverage, as shown in Table 2. EDC is formed on the large-sized clusters, which is consistent with the observed high activity of the catalysts with high loadings. It is noted that a certain fraction of $CuCl_2$ is also in the form of surface copper aluminate even for the large-sized cluster (i.e., the catalyst with high loadings), and it is nonreducible.

3.3.3. Size-Dependent Adsorption of Ethylene. Figure 6 reveals that the relationship between the interaction energy of ethylene and the cluster size features a volcano curve. Ethylene adsorption becomes weaker from the cluster with one $CuCl_2$ to the cluster of $(CuCl_2)_2$. Then, the interaction becomes stronger on the larger clusters ($(CuCl_2)_4$ > $(CuCl_2)_3$) on the γ-$Al_2O_3(100)$ surface. The cluster size dependence of ethylene on the γ-$Al_2O_3(110)$ surface follows a similar tendency on the (100) surface, except for a tiny difference between the interaction energy on the cluster $(CuCl_2)_3$ and the cluster $(CuCl_2)_4$ supported by the γ-$Al_2O_3(110)$ surface. In addition, the ethylene adsorption is stronger on $CuCl_2$ supported on γ-$Al_2O_3(110)$ than on the (100) surface, regardless of the cluster size. The significantly strong adsorption on the clusters $(CuCl_2)_3$ and $(CuCl_2)_4$ is due to the formation of EDC during the adsorption. Ethylene binds with the copper atom on smaller clusters (i.e., $CuCl_2$ and $(CuCl_2)_2$), and the charge transfer between the carbon atoms and the copper is observed in Figure 6.

The adsorption of ethylene on metal atoms follows the classic Dewar−Chatt donation/back-donation model.[35−37] On the one hand, the cupric ion has nine 9d electrons, and thus one d orbital available to accept electrons from ethylene; on the other hand, the electron can back-donate from a filled d orbital to the empty π^* orbital. The short d-band center (ε_d) of copper atoms was calculated to explain the size-dependent ethylene adsorption on the small-sized clusters (i.e., $CuCl_2$ and $(CuCl_2)_2$ on γ-$Al_2O_3(110)$ and (100)) since it was demonstrated to better characterize the reactivity of metal oxides and metal carbides compared to the infinite d-band center.[38,39] It is defined as $\varepsilon_d = \frac{\int \rho E dE}{\int \rho dE}$, where p is the density of states, E is the energy with respect to the Fermi level, and a cutoff of 1 Å was used in the calculation of the density of state. As illustrated in Figure 6, the weaker interaction energy between ethylene and the clusters can be attributed to the smaller short d-band center of Cu, since the shift-down of the short d-band center results in a more significant energy difference between the metal d orbitals and π^* orbitals and weakens the back-donation.

To explain the distinct adsorption modes for small-sized and large-sized clusters, we introduced a term named the formation energy of the Cl vacancy. The formation energy of the oxygen vacancy has been used in the studies of oxides to describe the oxidizing ability, and a smaller formation energy of oxygen

https://dx.doi.org/10.1021/acs.jpcc.9b11037
J. Phys. Chem. C 2020, 124, 10430−10440

vacancy means the surface is a better oxidant.[40] Metal oxides and metal chlorides are in the same class of catalysts, and they have a considerable similarity. Here, the formation energy of the chlorine vacancy ΔE_v is calculated as the reaction energy of the following reaction:

$$(CuCl_2)_n \rightarrow (CuCl_2)_{nv} + 1/2Cl_2(g)$$

where $(CuCl_2)_n$ is the chloride cluster and $(CuCl_2)_{nv}$ is the cluster with a chlorine vacancy on the surface. The most stable configurations of $(CuCl_2)_{nv}/\gamma$-$Al_2O_3(110)$ or (100) are shown in Figure S8, Supporting Information. It is found that the surface is highly dynamic, where Cl_1 migrates to the position of Cl_2 or Cl_3 after the optimization process if removing Cl_2 or Cl_3 from $(CuCl_2)_3$ in the initial configuration. It indicates the possibility of Cl migration on the catalyst surface.

The evolution of the formation energy of the Cl vacancy with the cluster size on two alumina surfaces is plotted in Figure 7a. The formation energy of the Cl vacancy (ΔE_v) gradually decreases with the increase of the cluster size on the (100) surface, while it decreases dramatically from $CuCl_2$ to $(CuCl_2)_3$ and then tends to be constant on the (110) surface. The intense interaction between $CuCl_2$ and the surface for the small clusters results in the high formation energy of the Cl vacancy. $CuCl_2$ and $(CuCl_2)_2$ clusters generate large ΔE_v, and thus, they are hard to be reduced. $(CuCl_2)_3$ and $(CuCl_2)_4$ clusters have a smaller ΔE_v as shown in Figure 7a, which means they are easily reduced. It is concluded that the size-dependent adsorption modes of ethylene are attributed to the size-dependent formation energy of the Cl vacancy. It means that making a smaller ΔE_v can result in a catalyst with higher oxidizing ability. Notably, the gas oxidant, such as oxygen, must be able to reoxidize the surface to complete the catalytic cycle. If the chlorine is too natural to remove from the surface, it will be challenging to get back. Therefore, it is suggested to follow "a medium principle", that is, modify the surface to get a moderate ΔE_v.

To find the underlying reason for the different ΔE_v, Bader charges of all the chlorine atoms in $(CuCl_2)_n$ are calculated. The average charge of the Cl atoms in the cluster models increases with the increment of the cluster size. The Cl atoms are less charged means less electron are transferred to the Cl atoms in the large cluster, which indicates the interaction between Cl and the neighboring atoms is weaker, and thus the Cl atom is easier to be removed. Thus, ethylene could extract two Cl atoms in the larger clusters, and the interaction energy becomes more negative from $(CuCl_2)_3$ to $(CuCl_2)_4$.

In Section 3.3.1, we explored the adsorption behavior of ethylene for the cases of two neighboring chlorine atoms with a distance of around 3.5 Å on the $(CuCl_2)_4/\gamma$-$Al_2O_3(110)$, and three distinct models were identified. Here, we analyzed the formation energy of each Cl vacancy and the Bader charge of each Cl atom to exploit the underlying reason. A linear relationship between the interaction energy between C_2H_4 and the clusters and the formation energy of the Cl vacancy is witnessed, as illustrated in Figure 7b. Notably, ΔE_v should be smaller to facilitate the migration of chlorine atoms from the surface to ethylene. Therefore, the site required for the highly oxidizing activity should have two neighboring chlorine atoms, and the formation energy of the Cl vacancy is small. The mapping of the ΔE_v of all the Cl atoms on $(CuCl_2)_4/\gamma$-$Al_2O_3(110)$ is displayed in the inset figure in Figure 7c. ΔE_v decreases with the color changes from red to blue, and the bluest chlorine atom displays the lowest formation energy of the Cl vacancy. The different colors demonstrate the heterogeneity of the surface. The formation energy of various Cl vacancies can be attributed to the distinct Bader charge of Cl.

4. CONCLUSIONS

In this paper, the interface structures of the $(CuCl_2)_n$ cluster on γ-$Al_2O_3(110)$ and γ-$Al_2O_3(100)$ were investigated first. It is found that the structures of both $CuCl_2$ and the alumina surface were distorted upon the adsorption of $CuCl_2$. The adsorption energy of $CuCl_2$ on γ-Al_2O_3 (110) gradually decreases with the increment of the cluster size. The adsorption of $(CuCl_2)_n$ clusters on γ-$Al_2O_3(110)$ is stronger than that on γ-Al_2O_3 (100), which is attributed to the stronger Lewis acidity of Al atoms on γ-$Al_2O_3(110)$.

Moreover, the adsorption of ethylene on $(CuCl_2)_n/\gamma$-$Al_2O_3(110)$ and $(CuCl_2)_n/\gamma$-$Al_2O_3(100)$ was examined, and the cluster-size-dependent adsorption mode was discovered. Ethylene sits on the top of one copper atom on the small-sized clusters (i.e., $CuCl_2$ and $(CuCl_2)_2$), while ethylene converts to EDC by extracting two chlorine atoms from the large-sized clusters (i.e., $(CuCl_2)_3$ and $(CuCl_2)_4$) for both γ-$Al_2O_3(110)$ and (100). The size-dependent adsorption modes of ethylene can be explained by the size-dependent formation energy of the Cl vacancy and the size-dependent Bader charge of Cl. The formation energy of the Cl vacancy decreases with the increase of the cluster size, which results in the strong oxidizing ability of the catalyst at high loadings.

It is concluded that the mechanism of ethylene adsorption depends on the cluster size or, more precisely, on the formation energy of the Cl vacancy. The interaction between ethylene and $CuCl_2$ changes from the Eley-Rideal mechanism on the large clusters with a low formation energy of the Cl vacancy to the Langmuir−Hinshword mechanism on the small clusters with a high formation energy of the Cl vacancy. The distinct Cl vacancy formation energy of each Cl atom in one cluster reflects the heterogeneity of the surface. A better catalyst could be developed by using different supports or adding promoters to tune the electronic structure and the formation energy of the Cl vacancy.

■ ASSOCIATED CONTENT

Supporting Information

The Supporting Information is available free of charge at https://pubs.acs.org/doi/10.1021/acs.jpcc.9b11037.

Unit cell vectors of the model; details of the calculations for the corresponding site coverage at different loadings and the TPR experiments; all possible configurations of $(CuCl_2)_n$ (n = 1−4) on γ-$Al_2O_3(110)$ and (100) and of ethylene adsorbing on $(CuCl_2)_n$ (n = 1−4) supported by γ-$Al_2O_3(110)$ and (100); adsorption configuration of ethylene on $(CuCl_2)_3/\gamma$-$Al_2O_3(110)$ and $(CuCl_2)_4/\gamma$-$Al_2O_3(110)$; TRP results; top views of the second ethylene adsorbed on the clusters supported on the γ-$Al_2O_3(110)$ surface; comparison of the interaction energy of the second ethylene and the first ethylene on the cluster supported on γ-$Al_2O_3(110)$; configurations of $(CuCl_2)_n$−Cl (n = 3−4) on γ-$Al_2O_3(110)$ and (100) surfaces; comparison of the adsorption energy of $CuCl_2$ on γ-$Al_2O_3(110)$ (PDF)

https://dx.doi.org/10.1021/acs.jpcc.9b11037
J. Phys. Chem. C 2020, 124, 10430−10440

AUTHOR INFORMATION

Corresponding Author

De Chen − *Department of Chemical Engineering, Norwegian University of Science and Technology, N-7491 Trondheim, Norway;* orcid.org/0000-0002-5609-5825; Email: de.chen@ntnu.no

Authors

Yanying Qi − *Department of Chemical Engineering, Norwegian University of Science and Technology, N-7491 Trondheim, Norway*

Endre Fenes − *Department of Chemical Engineering, Norwegian University of Science and Technology, N-7491 Trondheim, Norway;* orcid.org/0000-0001-9003-552X

Hongfei Ma − *Department of Chemical Engineering, Norwegian University of Science and Technology, N-7491 Trondheim, Norway*

Yalan Wang − *Department of Chemical Engineering, Norwegian University of Science and Technology, N-7491 Trondheim, Norway*

Kumar Ranjan Rout − *Department of Chemical Engineering, Norwegian University of Science and Technology, N-7491 Trondheim, Norway; SINTEF Industry, Trondheim, Norway*

Terje Fuglerud − *INOVYN, Porsgrunn, Norway*

Marco Piccinini − *INOVYN, 5190 Jemeppe-sur-Sambre, Belgium*

Complete contact information is available at: https://pubs.acs.org/10.1021/acs.jpcc.9b11037

Notes

The authors declare no competing financial interest.

ACKNOWLEDGMENTS

The financial support from the Centre for Industrial Catalysis Science and Innovation (iCSI), which receives financial support from the NO-237922 Research Council of Norway, is gratefully acknowledged. The computational time provided by the Notur project NN4685K is highly acknowledged.

REFERENCES

(1) Scharfe, M.; Lira-Parada, P. A.; Paunovic, V.; Moser, M.; Amrute, A. P.; Perez-Ramirez, J. Oxychlorination-Dehydrochlorination Chemistry on Bifunctional Ceria Catalysts for Intensified Vinyl Chloride Production. *Angew. Chem., Int. Ed.* **2016**, *55*, 3068−3072.

(2) Schirmeister, R.; Kahsnitz, J.; Trager, M. Influence of EDC Cracking Severity on the Marginal Costs of Vinyl Chloride Production. *Ind. Eng. Chem. Res.* **2009**, *48*, 2801−2809.

(3) Zhong, J. W.; Xu, Y. P.; Liu, Z. M. Heterogeneous Non-Mercury Catalysts for Acetylene Hydrochlorination: Progress, Challenges, and Opportunities. *Green Chem.* **2018**, *20*, 2412−2427.

(4) Go, K. S.; Kim, Y.; Real Son, S.; Kim, S. D. 1,2-Dichloroethane Production by Two-Step Oxychlorination Reactions in a Fluidized Bed Reactor. *Chem. Eng. Sci.* **2010**, *65*, 499−503.

(5) Leofanti, G.; Marsella, A.; CremaschI, B.; Garilli, M.; Zecchina, A.; Spoto, G.; Bordiga, S.; Fisicaro, P.; Prestipino, C.; Villain, F.; Lamberti, C. Alumina-Supported Copper Chloride: 4. Effect of Exposure to O_2 and HCl. *J. Catal.* **2002**, *205*, 375−381.

(6) Leofanti, G.; Marsella, A.; Cremaschi, B.; Garilli, M.; Zecchina, A.; Spoto, G.; Bordiga, S.; Fisicaro, P.; Berlier, G.; Prestipino, C.; et al. Alumina-Supported Copper Chloride 3. Effect of Exposure to Ethylene. *J. Catal.* **2001**, *202*, 279−295.

(7) Finocchio, E.; Rossi, N.; Busca, G.; Padovan, M.; Leofanti, G.; Cremaschi, B.; Marsella, A.; Carmello, D. Characterization and Catalytic Activity of $CuCl_2$-Al_2O_3 ethylene Oxychlorination Catalysts. *J. Catal.* **1998**, *179*, 606−618.

(8) Rout, K. R.; Fenes, E.; Baidoo, M. F.; Abdollahi, R.; Fuglerud, T.; Chen, D. Highly Active and Stable CeO_2-Promoted $CuCl_2/Al_2O_3$ Oxychlorination Catalysts Developed by Rational Design Using a Rate Diagram of the Catalytic Cycle. *ACS Catal.* **2016**, *6*, 7030−7039.

(9) Gianolio, D.; Muddada, N. B.; Olsbye, U.; Lamberti, C. Doped-$CuCl_2/Al_2O_3$ Catalysts for Ethylene Oxychlorination: Influence of Additives on the Nature of Active Phase and Reducibility. *Nucl. Instrum. Methods Phys. Res., Sect. B* **2012**, *284*, 53−57.

(10) Muddada, N. B.; Olsbye, U.; Leofanti, G.; Gianolio, D.; Bonino, F.; Bordiga, S.; Fuglerud, T.; Vidotto, S.; Marsella, A.; Lamberti, C. Quantification of Copper Phases, Their Reducibility and Dispersion in Doped- $CuCl_2/Al_2O_3$ Catalysts for Ethylene Oxychlorination. *Dalton Trans.* **2010**, *39*, 8437−8449.

(11) Lamberti, C.; Prestipino, C.; Bonino, F.; Capello, L.; Bordiga, S.; Spoto, G.; Zecchina, A.; Moreno, S. D.; Cremaschi, B.; Garilli, M.; et al. The Chemistry of the Oxychlorination Catalyst: An in Situ, Time-Resolved Xanes Study. *Angew. Chem., Int. Ed.* **2002**, *41*, 2341−2344.

(12) Prestipino, C.; Bordiga, S.; Lamberti, C.; Vidotto, S.; Garilli, M.; Cremaschi, B.; Marsella, A.; Leofanti, G.; Fisicaro, P.; Spoto, G.; et al. Structural Determination of Copper Species on the Alumina-Supported Copper Chloride Catalyst: A Detailed EXAFS Study. *J. Phys. Chem. B* **2003**, *107*, 5022−5030.

(13) Muddada, N. B.; Olsbye, U.; Caccialupi, L.; Cavani, F.; Leofanti, G.; Gianolio, D.; Bordiga, S.; Lamberti, C. Influence of Additives in Defining the Active Phase of the Ethylene Oxychlorination Catalyst. *Phys. Chem. Chem. Phys.* **2010**, *12*, 5605−5618.

(14) Leofanti, G.; Padovan, M.; Garilli, M.; Carmello, D.; Zecchina, A.; Spoto, G.; Bordiga, S.; Palomino, G. T.; Lamberti, C. Alumina-Supported Copper Chloride: 1. Characterization of Freshly Prepared Catalyst. *J. Catal.* **2000**, *189*, 91−104.

(15) Leofanti, G.; Padovan, M.; Garilli, M.; Carmello, D.; Marra, G. L.; Zecchina, A.; Spoto, G.; Bordiga, S.; Lamberti, C. Alumina-Supported Copper Chloride: 2. Effect of Aging and Thermal Treatments. *J. Catal.* **2000**, *189*, 105−116.

(16) Vajglová, Z.; Kumar, N.; Eränen, K.; Tokarev, A.; Peurla, M.; Peltonen, J.; Murzin, D. Y.; Salmi, T. Influence of the Support of Copper Catalysts on Activity and 1,2-Dichloroethane Selectivity in Ethylene Oxychlorination. *Appl. Catal., A* **2018**, *556*, 41−51.

(17) Digne, M.; Sautet, P.; Raybaud, P.; Euzen, P.; Toulhoat, H. Use of DFT to Achieve a Rational Understanding of Acid−Basic Properties of Γ-Alumina Surfaces. *J. Catal.* **2004**, *226*, 54−68.

(18) Digne, M.; Sautet, P.; Raybaud, P.; Euzen, P.; Toulhoat, H. Hydroxyl Groups on Γ-Alumina Surfaces: A DFT Study. *J. Catal.* **2002**, *211*, 1−5.

(19) Louwerse, M. J.; Rothenberg, G. Modeling Catalyst Preparation: The Structure of Impregnated−Dried Copper Chloride on Γ-Alumina at Low Loadings. *ACS Catal.* **2013**, *3*, 1545−1554.

(20) Rout, K. R.; Baidoo, M. F.; Fenes, E.; Zhu, J.; Fuglerud, T.; Chen, D. Understanding of Potassium Promoter Effects on Oxychlorination of Ethylene by Operando Spatial-Time Resolved Uv−Vis−Nir Spectrometry. *J. Catal.* **2017**, *352*, 218−228.

(21) Neurock, M.; Zhang, X.; Olken, M.; Jones, M.; Hickman, D.; Calverley, T.; Gulotty, R. A First-Principle Analysis of Ethylene Chemisorption on Copper Chloride Clusters. *J. Phys. Chem. B* **2001**, *105*, 1562−1572.

(22) Wellendorff, J.; Lundgaard, K. T.; Mogelhoj, A.; Petzold, V.; Landis, D. D.; Norskov, J. K.; Bligaard, T.; Jacobsen, K. W. Density Functionals for Surface Science: Exchange-Correlation Model Development with Bayesian Error Estimation. *Phys. Rev. B: Condens. Matter Mater. Phys.* **2012**, *85*, 235149.

(23) Kresse, G.; Furthmuller, J. Efficiency of Ab-Initio Total Energy Calculations for Metals and Semiconductors Using a Plane-Wave Basis Set. *Comput. Mater. Sci.* **1996**, *6*, 15−50.

(24) Kresse, G.; Hafner, J. Ab Initio Molecular Dynamics for Liquid Metals. *Phys. Rev. B: Condens. Matter Mater. Phys.* **1993**, *47*, 558−561.

(25) Kresse, G.; Hafner, J. Ab Initio Molecular Dynamics for Open-Shell Transition Metals. *Phys. Rev. B: Condens. Matter Mater. Phys.* **1993**, *48*, 13115−13118.

(26) Kresse, G.; Joubert, D. From Ultrasoft Pseudopotentials to the Projector Augmented-Wave Method. *Phys. Rev. B: Condens. Matter Mater. Phys.* **1999**, *59*, 1758−1775.
(27) Mei, D.; Ge, Q.; Kwak, J. H.; Kim, D. H.; Szanyi, J.; Peden, C. H. F. Adsorption and Formation of Bao Overlayers on Γ-Al_2O_3 Surfaces. *J. Phys. Chem. C* **2008**, *112*, 18050−18060.
(28) Henkelman, G.; Arnaldsson, A.; Jónsson, H. A Fast and Robust Algorithm for Bader Decomposition of Charge Density. *Comput. Mater. Sci.* **2006**, *36*, 354−360.
(29) Sanville, E.; Kenny, S. D.; Smith, R.; Henkelman, G. Improved Grid-Based Algorithm for Bader Charge Allocation. *J. Comput. Chem.* **2007**, *28*, 899−908.
(30) Momma, K.; Izumi, F. Vesta 3 for Three-Dimensional Visualization of Crystal, Volumetric and Morphology Data. *J. Appl. Crystallogr.* **2011**, *44*, 1272−1276.
(31) Hammer, B. a. H. L. B.; Nørskov, J. K.; Hansen, L. B. Improved Adsorption Energetics within Density-Functional Theory Using Revised Perdew-Burke-Ernzerhof Functionals. *Phys. Rev. B: Condens. Matter Mater. Phys.* **1999**, *59*, 7413−7421.
(32) Cholewinski, M. C.; Dixit, M.; Mpourmpakis, G. Computational Study of Methane Activation on Γ-Al_2O_3. *ACS Omega.* **2018**, *3*, 18242−18250.
(33) Jenness, G. R.; Christiansen, M. A.; Caratzoulas, S.; Vlachos, D. G.; Gorte, R. J. Site-Dependent Lewis Acidity of γ-Al_2O_3 and Its Impact on Ethanol Dehydration and Etherification. *J. Phys. Chem. C* **2014**, *118*, 12899−12907.
(34) Digne, M.; Raybaud, P.; Sautet, P.; Guillaume, D.; Toulhoat, H. Atomic Scale Insights on Chlorinated Γ-Alumina Surfaces. *J. Am. Chem. Soc.* **2008**, *130*, 11030−11039.
(35) Chatt, J.; Duncanson, L. A. Olefin Co-Ordination Compounds. Part Iii. Infra-Red Spectra and Structure: Attempted Preparation of Acetylene Complexes. *J. Chem. Soc.* **1953**, 2939−2947.
(36) Xia, Z.; Zhang, S.; Liu, F.; Ma, Y.; Qu, Y.; Wu, C. Size-Dependent Adsorption of Styrene on Pd Clusters: A Density Functional Theory Study. *J. Phys. Chem. C* **2019**, *123*, 2182−2188.
(37) Chatt, J.; Duncanson, L. A.; Venanzi, L. M. Directing Effects in Inorganic Substitution Reactions. Part I. A Hypothesis to Explain the Trans-Effect. *J. Chem. Soc.* **1955**, 4456−4460.
(38) Kitchin, J. R.; Nørskov, J. K.; Barteau, M. A.; Chen, J. G. Trends in the Chemical Properties of Early Transition Metal Carbide Surfaces: A Density Functional Study. *Catal. Today* **2005**, *105*, 66−73.
(39) Wei, Z.-Z.; Li, D.-C.; Pang, X.-Y.; Lv, C.-Q.; Wang, G.-C. The Mechanism of Low-Temperature CO Oxidation on IB Group Metals and Metal Oxides. *ChemCatChem* **2012**, *4*, 100−111.
(40) McFarland, E. W.; Metiu, H. Catalysis by Doped Oxides. *Chem. Rev.* **2013**, *113*, 4391−4427.

https://dx.doi.org/10.1021/acs.jpcc.9b11037
J. Phys. Chem. C 2020, 124, 10430−10440